Experimental Animals
Exp. Anim. 75(1), 23–39, 2026

Original

Exploring the role of zolpidem in alleviating cognitive and motor impairments in chronic cerebral hypoperfusion: a rat model study with *in vivo* and *in silico* insights

Sherilyn M.T. CHOO[1)], Fatin H. MOHAMAD[1,2)], Syarifah Maisarah Sayed MOHAMAD[1)], Jafri Malin ABDULLAH[1)], Khairul Bariyyah Abd HALIM[3)], Azzmer Azzar Abdul HAMID[4)] and Ahmad Tarmizi CHE HAS[1)]

[1)]*Department of Neurosciences, School of Medical Sciences, Health Campus, Universiti Sains Malaysia, Kubang Kerian, 16150 Kota Bharu, Kelantan, Malaysia*
[2)]*Cytogenetics and Molecular Labs (CMDL), Premier Integrated Labs Sdn. Bhd, Pantai Hospital Kuala Lumpur, Jalan Bukit Pantai, Bangsar, 59100 Kuala Lumpur, Malaysia*
[3)]*Research Unit for Bioinformatics and Computational Biology (RUBIC), Kulliyyah of Science, International Islamic University Malaysia, Jalan Sultan Ahmad Shah, Bandar Indera Mahkota, 25200 Kuantan, Pahang, Malaysia*
[4)]*Department of Biotechnology, Kulliyyah of Science, International Islamic University Malaysia, Jalan Sultan Ahmad Shah, Bandar Indera Mahkota, 25200 Kuantan, Pahang, Malaysia*

Abstract: The ε-containing GABA(A) receptors (GABAARs), a lesser-studied subtype within the GABAAR family, have garnered attention due to their distinct pharmacological properties and potential involvement in brain injury. Zolpidem (ZPM), a widely used Z-drug, is known to induce paradoxical effects in patients with brain injury, although the underlying molecular mechanisms remain unclear. In this study, a chronic cerebral hypoperfusion (CCH) rat model was established using Permanent Bilateral Occlusion of the Common Carotid Arteries (PBOCCA), followed by administration of ZPM at doses of 1.0, 2.0, and 4.0 mg/kg. Behavioral assessments demonstrated that the 1.0 mg/kg dose of ZPM significantly improved spatial learning and memory acquisition (P<0.01) and enhanced memory retention (P<0.001), whereas higher doses resulted in sedation and cognitive impairment. Immunohistochemical analysis revealed an upregulation of the ε subunit expression in the hippocampal CA1 and CA3 regions of CCH rats (P<0.05), suggesting alterations in receptor composition in response to cerebral hypoperfusion. Further investigation of ZPM's interaction with ε-containing GABAARs (specifically the α1β2ε subtype) was conducted using *in silico* techniques. Molecular docking identified the α1+/ε- binding interface as a favorable ZPM binding site, with key residues being either conserved or suitably replaced. Molecular dynamics simulations demonstrated that ZPM stabilizes the receptor while permitting conformational flexibility, consistent with its role as a positive allosteric modulator. These findings provide evidence that ZPM interacts with ε-containing GABAARs, potentially explaining its paradoxical effects observed in brain injury models.
Key words: chronic cerebral hypoperfusion (CCH), GABA(A) receptors (GABAARs), *in silico*, *in vivo*, zolpidem

Introduction

Zolpidem (ZPM) is a potent sedative-hypnotic agent primarily prescribed for the management of insomnia [1]. As a non-benzodiazepine (non-BZD) derivative, ZPM functions as a positive allosteric modulator (PAM) of GABA(A) receptors (GABAARs) [2]. ZPM exhibits a high affinity for the α1 subunit of GABAARs, inter-

(Received 28 March 2025 / Accepted 10 July 2025 / Published online in J-STAGE 17 July 2025)
Corresponding author: A.T.C. Has. e-mail: ahmadtarmizi@usm.my

mediate affinity for the α2 and α3 subunits, and minimal affinity for the α5 subunit [2]. Pharmacologically, the α1 subunit is primarily responsible for mediating sedative effects, while the α2 and α3 subunits contribute to anxiolytic, anticonvulsant, myorelaxant, and ataxic effects [1]. The selective binding of ZPM to the α1 subunit enhances its efficacy in inducing sleep while minimizing adverse effects compared to traditional BZDs, making it a preferred treatment for sleep disorders [3]. Despite its sedative properties, ZPM has been reported to induce wakefulness in patients with various brain injuries, including trauma, stroke, and disorders of consciousness (DOC) [4–6]. This phenomenon extends to recovery following hypoxic damage, cerebrovascular ischemic injury, central nervous system (CNS) infections, toxin exposure, degenerative diseases, tumors, and congenital disorders [4, 7–9]. The paradoxical awakening effect of ZPM, which contrasts with its intended sedative-hypnotic action, is believed to arise from its interaction with GABAARs, suggesting a shift in neurotransmission polarity under pathological conditions.

Recent studies have highlighted ZPM's potential to enhance cognitive functions and neuroplasticity, particularly in ischemic stroke recovery in rat models [10]. Cognitive functions, often attributed to the hippocampus, rely on α5-containing GABAARs, which are involved in spatial learning, memory, and other cognitive processes [11, 12]. Although α5-containing GABAARs account for only about 5% of GABAARs in the CNS, they represent nearly 25% of hippocampal GABAARs [13]. Interestingly, ZPM does not significantly affect these receptors, suggesting that its cognitive-enhancing effects do not involve the α5 subunit.

The paradoxical effects of ZPM may result from altered GABAergic transmission following pathological insults such as ischemia or neurodegeneration. These conditions are known to disrupt chloride homeostasis, leading to elevated intracellular chloride ion (Cl^-) levels and causing GABAAR activation to elicit depolarizing, excitatory responses rather than the typical inhibitory effects [14]. This shift in GABAergic signalling suggests that non-canonical GABAAR subtypes, possibly acting through alternative binding mechanisms, may mediate these aberrant responses. Notably, several studies have reported alterations in GABAAR subunit composition under such pathological conditions [15–20]. Among these, the ε subunit—one of the most recently identified GABAAR subunits—has attracted attention due to its distinct biophysical and pharmacological properties. These unique characteristics may render ε-containing GABAARs particularly susceptible to modulation by ZPM, thereby potentially contributing to its paradoxical effects in disease states.

The ε subunit is predominantly localized in brain regions such as the amygdala, hippocampus, locus coeruleus, hypothalamus, and subthalamus [21, 22]. In contrast to other GABAAR subtypes, ε-containing receptors exhibit rapid desensitization, reduced sensitivity to Zn^{2+}, and smaller GABA-mediated current amplitudes [21–26]. Even in the absence of GABA, ε-containing receptors preferentially adopt an open ionophore state, leading to leakage currents [25]. This dynamic may help explain the transient motor and cognitive improvements observed in patients with brain injuries treated with ZPM, suggesting that ε subunit upregulation plays a key role in mediating these paradoxical outcomes. The present study aims to investigate the binding of ZPM to ε-containing GABAARs and explore the mechanisms underlying this interaction. To address this, a chronic cerebral hypoperfusion (CCH) rat model induced by Permanent Bilateral Occlusion of the Common Carotid Arteries (PBOCCA) was employed, representing a model for vascular cognitive impairment and neurodegenerative diseases. Rats were administered varying doses of ZPM, and their locomotor, learning, and memory abilities were assessed using the Morris water maze (MWM) and open-field test (OFT). Immunohistochemical analyses were performed on the hippocampal CA1 and CA3 regions to quantify the expression of the ε subunit. The ε-containing GABAAR was modelled and docked with ZPM, and molecular dynamics simulations were conducted to elucidate the structural and ligand interactions that contribute to ZPM binding to these receptors.

Materials and Methods

Animal quarantine and acclimatization

The animal experiments were conducted in accordance with the guidelines approved by the Universiti Sains Malaysia (USM) Institutional Animal Care and Use Committee (USM IACUC): USM/IACUC/2024/(145)(1310). Male Sprague-Dawley (SD) rats, weighing between 200 and 250 g, were obtained from the Animal Research and Service Centre. The rats were acclimatized in an animal quarantine room for a minimum of one week before any experimental procedures were initiated. During this period, food and water were provided *ad libitum*, and the rats were maintained on a 12-h light/dark cycle under constant temperature conditions.

Induction of chronic cerebral hypoperfusion via permanent bilateral occlusion of the common carotid arteries

Chronic cerebral hypoperfusion was induced by permanently occluding both common carotid arteries in rats, a well-established method for creating significant deficits in hippocampal neurons. This model results in reduced cerebral blood flow but does not completely deprive the brain of oxygen, as collateral blood supply from other arteries remains intact [27]. Each rat was anesthetized with a mixture of ketamine (80 mg/kg; Troy Laboratories Pty Ltd., Glendenning, Australia) and xylazine (10 mg/kg; Troy Laboratories Pty Ltd.) administered via intraperitoneal injection. Following anesthesia, rats were randomly assigned to one of five treatment groups, each consisting of at least six rats, based on a previous study: Sham + saline (control), CCH + saline (untreated CCH), CCH + 1.00 mg/kg ZPM (LGC Standards Ltd., Teddington, UK), CCH + 2.00 mg/kg ZPM, and CCH + 4.00 mg/kg ZPM [10].

Automated open-field test

Spontaneous locomotor activity was assessed using an automated OFT (Panlab, Barcelona, Spain). This experiment allowed the evaluation of the effects of ZPM on anxiety levels and locomotor activity following PBOCCA surgery. The apparatus consisted of a Perspex glass enclosure (20 × 45 × 45 cm) with the floor divided into five zones. Infrared beams along the sides of the apparatus detected and recorded the movements and activities of each rat, which were then analyzed using ActiTrack software (Panlab). Each rat was placed in the center of the open field and allowed to habituate for 10 min before the recording session began. ZPM was administered via intraperitoneal injection 30 min prior to the recording, which lasted for 20 min. The floor of the open field was cleaned with 70% ethanol between rat trials to prevent cross-contamination.

MWM

The MWM test, a widely used tool to assess hippocampal-dependent learning and memory [28], was performed in a circular pool (74 cm height, 180 cm diameter, 551 cm circumference). The pool was divided into four quadrants—north, east, south, and west—with a plastic platform placed in the northwest quadrant. The platform, which was 50 cm high and 10 cm in diameter, was submerged 2 cm below the water surface. To obscure the platform from view, the water was made opaque by adding white water-based paint. The water temperature was maintained at 25°C throughout the experiment. The experiment began with a habituation day, during which rats' swimming abilities were assessed without the hidden platform. Each rat was allowed to swim for 60 s. Rats exhibiting significant difficulty in swimming were excluded from the study. Following habituation, the platform was introduced in the northwest quadrant, and rats underwent four daily trials over four consecutive days. Each trial involved releasing the rat from one of four randomized starting points, allowing up to 60 s to locate and climb onto the platform. Escape latency was recorded using SMART video-tracking software, and a stopwatch was used in parallel as a manual backup to ensure data accuracy and reliability. If a rat failed to locate the platform within 60 s, the trial was terminated, and the rat was guided to the platform using a stick and required to remain on it for at least 15 s before beginning the next trial. After the completion of the four daily trials, rats were administered an intraperitoneal injection of the respective drug to consolidate memory. Following the training phase, a probe trial was conducted in which the hidden platform was removed. The rats were released from a single point (S) and allowed to swim for 60 s. The latency for each rat to reach the target quadrant (NW) and the percentage of time spent in this quadrant were recorded and analyzed. No drug was administered after the probe trial. On the following day, a visible platform test was conducted, where the platform was placed in the southwest quadrant, raised 1 cm above the water surface to make it visible. Rats were released from a single point (E) and given a maximum of 60 s to locate and climb onto the platform, where they were required to remain for at least 15 s. This procedure was repeated twice. Data from the probe trial were analyzed using SMART analysis software v.3.0.05 (Panlab).

Immunohistochemistry

Immunohistochemical staining was performed following the protocol outlined by [29], with minor modifications. To ensure the exclusive presence of hippocampal tissue on the slides, tissue sections were initially deparaffinized by immersing the slides in xylene (R&M Chemicals, Petaling Jaya, Malaysia) twice for 3 min each. They were then rehydrated through a series of graded ethanol solutions (100, 90, 80, and 70%), with each solution applied for 3 min. Residual ethanol was removed by rinsing the slides under running tap water for 2–3 min. For antigen retrieval, the sections were immersed in a citrate-based retrieval solution and heated in a microwave at medium-high power for 12 min. After cooling to room temperature, the slides were rinsed twice in phosphate-buffered saline (PBS; Sigma-Aldrich, St. Louis, MO, USA) with gentle agitation for 5 min each. To block non-specific binding and reduce back-

ground staining, the sections were incubated with 3% normal goat serum (NGS; Sigma-Aldrich) for 2 h at room temperature. The slides were then washed with PBS and incubated overnight at 4°C in a humidified chamber with primary antibody targeting ε subunit (1:100 dilution). The following day, the slides were rinsed in PBS with gentle agitation for 5 min. The sections were then incubated with fluorophore-conjugated secondary antibody (goat anti-mouse; Abcam Ltd., Cambridge, UK), for 2 h at room temperature. To minimize photobleaching, all subsequent steps were performed under minimal light exposure. After incubation with secondary antibody, the slides were rinsed again in PBS, dried gently, and mounted with Fluoroshield™ containing 4',6'-diamidino-2-phenylindole (DAPI; Sigma-Aldrich) for nuclear counterstaining. Coverslips were applied, and the slides were allowed to dry at room temperature. Finally, the slides were stored at 4°C overnight before imaging with a fluorescence microscope.

Image analysis and quantification

Images were captured using an Olympus BX41 microscope (BX41, Olympus Corp., Tokyo, Japan), coupled with Olympus cellSens imaging software (version cellSens2.2_RU-_01, Olympus Corp.). The system was equipped with a mercury vapor bulb (U-RFL-T, Olympus Corp.) for fluorescence imaging, with excitation wavelengths set to 358 nm (blue), 488 nm (green), and 594 nm (red). Images were acquired at 40× magnification, with an exposure time of 450 ms for both the red and green channels. The imaging area for each acquisition was standardized at 550.399 μm^2. Quantitative analysis of integrated density was performed on images from the CA1 and CA3 regions of the hippocampus using ImageJ software (ImageJ 1.53c, National Institute of Health, Bethesda, MD, USA). Integrated density values were averaged for each region across the respective slides. Respective haematoxylin and DAPI nuclear staining were used to identify the hippocampal regions of interests (ROIs) [CA1 and CA3] (Supplementary Figs. 1 and 2).

Statistical analysis

Statistical analyses for the MWM, OFT and immunofluorescence studies were performed using GraphPad Prism9 (Version 9.0.1, GraphPad Software Inc., San Diego, CA, USA). All datasets were tested for Gaussian distribution using the Shapiro-Wilk normality test prior to parametric analysis. For comparisons involving two groups, unpaired *t*-test was used, for three or more groups, ordinary one-way ANOVA was used, with Tukey's post-hoc analysis for multiple comparisons. For the four-day MWM training data comparison, a repeated two-way ANOVA was used with Tukey's post-hoc multiple comparisons. All data are plotted as mean values, with error bars representing the standard deviation. The significance level was set at $P<0.05$.

Homology modelling of ε-containing $GABA_AR$

The crystallographic structure of the α1β2γ2 GABAAR bound to GABA and allopregnanolone (RCSB PDB ID: 8SI9) [30] was used as the template for constructing the α1β2ε GABAAR variant. This α1β2γ2 subtype was selected because it is the most predominant subtype of GABAARs in the CNS [13]. Prior to homology modelling, all non-receptor elements, including heavy chains, light chains, and ligands, were removed from the template using PyMOL (version 2.5, Schrödinger Inc., NY, USA). The α1, β2, and ε subunit structures were retrieved from AlphaFold (DeepMind Technologies Ltd., London, UK) and aligned to their corresponding template chains in PyMOL. The γ2 subunit in the template was substituted with the ε subunit to create the alternative α1+/ε- binding interface, while preserving the canonical GABA-binding sites at the β2+/α1- interfaces [31]. The individual subunit sequences from the modelled receptor were extracted using locally written script. Multiple sequence alignment (MSA) was performed using Clustal Omega to compare the sequences of the template and modelled subunits. Homology modelling was then conducted using MODELLER 10.4, generating multiple structural models [32]. The best model was selected based on the lowest Discrete Optimized Protein Energy (DOPE) score. Structural validation was performed through Ramachandran plot analysis to assess steric hindrances and potential structural deviations that could impact subsequent molecular docking and simulation procedures.

Molecular docking

The 3D structure of ZPM was retrieved from the PubChem database. Since the cryo-EM structure used for homology modelling lacked hydrogen atoms due to its 1 Å resolution limit [33], hydrogen atoms were manually added to the receptor. The receptor and ligand .pdb files were subsequently converted into .pdbqt format, which is required for docking simulations in AutoDock 4.2. Molecular docking was performed using AutoDock 4.2 [34]. Targeted docking was done by adjusting grid box parameters to cover the extracellular α1+/ε- interface. Docking simulations generated nine potential binding poses for each ligand, with binding affinities estimated as free energy of binding (ΔG, kcal/mol). The best docking pose was selected based on the lowest binding energy and optimal spatial positioning within the α1+/ε-

interface. Molecular interactions, including hydrogen bonds, hydrophobic contacts, and π-π interactions, were analyzed using PyMOL [35], Protein-Ligand Interaction Profiler (PLIP) [36], and BIOVIA Discovery Studio [37].

Molecular dynamics simulation

Molecular dynamics (MD) simulations were performed using the GROMACS program in three stages: energy minimization, equilibration, and production [38]. Prior to MD simulation, receptor-ligand complex was superimposed with two GABA molecules at the β2+/α1- interfaces to ensure a more physiologically relevant simulation system. The modified receptor-ligand complexes were uploaded to CHARMM-GUI via the "Ligand Reader and Modeller" module to generate the relevant ligand topology and parameter files, which were incorporated into the receptor file.

Generation of lipid bilayer membrane using CHARMM-GUI

The receptor-ligand complex was uploaded to CHARMM-GUI and embedded into a lipid bilayer system following the protocol of [39]. The complex was aligned along the z-axis to ensure proper integration with the transmembrane domain. The system was embedded in a 1-Palmitoyl-2-Oleoyl-sn-Glycero-3-Phosphatidylcholine (POPC) lipid bilayer and solvated using TIP3P water molecules via the replacement method. POPC was chosen due to its physiological relevance as one of the most abundant phospholipids in mammalian cell membranes [40, 41]. It has been widely validated for simulating neurotransmitter receptors, demonstrating stability and structural relevance in mimicking biological membranes [40, 42–44]. Additionally, POPC is compatible with CHARMM-GUI and GROMACS simulations due to its well-parameterized force fields, allowing seamless integration into the CHARMM36 force field [45]. The simulation box was defined as a rectangular shape with x- and y-axes dimensions of 190, while the z-axis was adjusted to accommodate a 22.5 water molecule thickness at both the top and bottom layers. The temperature was set to 310.15 K, and Na^+ and Cl^- ions were added to neutralize the overall charge, achieving a final ion concentration of 0.15 M. GROMACS-compatible simulation files, including coordinate, parameter, and topology files, were generated.

Minimization, equilibration, and production stages

For each system, energy minimization was performed using 5,000 steps of the steepest descent algorithm until the energy level reached below 1,000 kJ mol^{-1}. During the equilibration phase, a five-step isothermal-isochoric (NVT) ensemble was conducted, consisting of three 125 ps steps followed by two 500 ps steps, during which the number of particles (N), volume (V), and temperature (T) were kept constant to achieve thermal equilibration. This was followed by an isothermal-isobaric (NPT) ensemble, where the number of particles (N), pressure (P), and temperature (T) were maintained constant while the volume was adjusted to stabilize the system under constant pressure [46]. Subsequently, a 100 ns MD production run was performed for all systems to analyze receptor-ligand interactions and system stability over time, corresponding to 50,000,000 ps of simulation steps with a time step of 0.002 fs. The files generated by CHARMM-GUI were triplicated using different initial velocities, which was calculated using different random gen seed value for each of the replica, to generate three independent MD simulations to enhance result reliability and minimize biases. Various stability assessments and analyses were then conducted using the tools available in the GROMACS suite.

Results

Chronic cerebral hypoperfusion: effects of zolpidem on locomotion

The OFT is widely used to evaluate motor function in animal models [47]. In the present study, we assessed the locomotor function of rats with CCH following ischemic injury, comparing them with control rats that did not undergo CCH. ZPM was administered to the CCH-treated rats 20 min prior to the test to ensure optimal drug efficacy. We measured locomotor function using total activity, total distance traveled, and movement speed. Rats treated with ZPM at doses of 2.0 mg/kg and 4.0 mg/kg exhibited significantly reduced locomotor activity compared to untreated CCH rats ($P<0.01$ and $P<0.001$, respectively; Fig. 1, Top). Similarly, the total distance traveled by the ZPM-treated rats in the OFT was significantly lower than that of untreated CCH rats ($P<0.05$ and $P<0.001$, respectively; Fig. 1, Middle). Movement speed was also significantly reduced in rats treated with 4.0 mg/kg ZPM ($P<0.001$, Fig. 1, Below).

Chronic cerebral hypoperfusion: effects of zolpidem on anxiety-like and exploratory behaviors

Anxiety can influence locomotor function, particularly in unfamiliar environments such as the OFT. To assess the impact of ischemic injury and ZPM treatment on anxiety and exploratory behaviors, we analyzed the time spent in the center of the field and the number of rearing events during the OFT. Compared to untreated CCH rats, sham rats spent significantly lower time in the center of

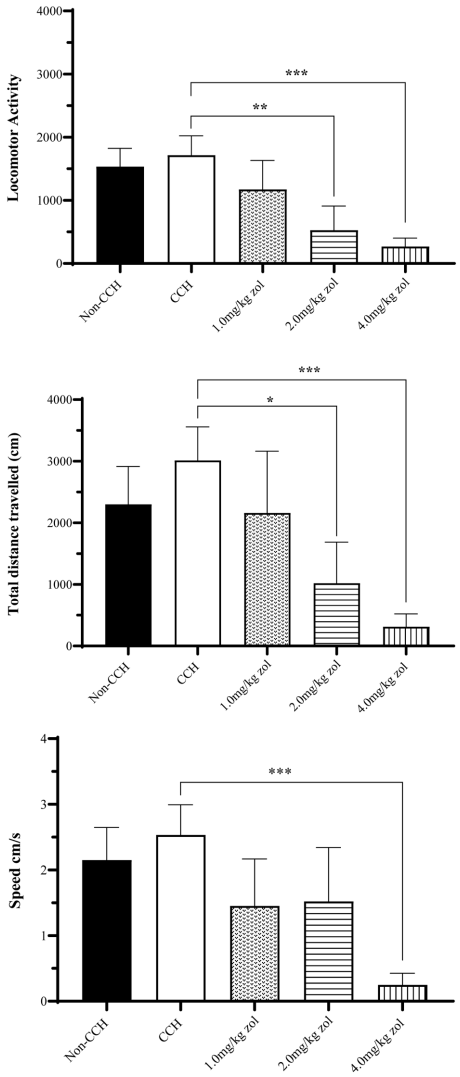

Fig. 1. Effects of zolpidem on the total locomotor activity in open-field test after two weeks recovery period (Top). (***P*<0.01, *** *P*<0.001; compared to the non-treated CCH group). Effects of zolpidem on the total distance travelled by the animals during the open-field test (Middle). (**P*<0.05, ****P*<0.001; compared to the non-treated CCH group). Effects of zolpidem on the speed of the animals during open-field test (Below). (****P*<0.001; compared to the non-treated CCH group). One-way ANOVA was used to assess the effects of group. Number of animals used for each group=6.

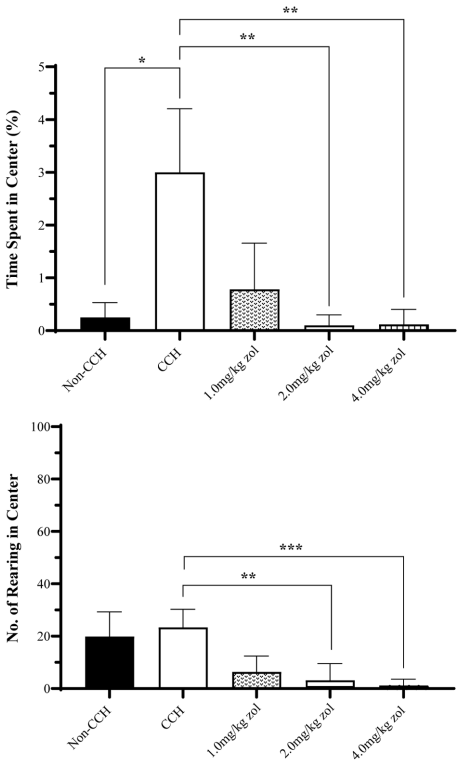

Fig. 2. Evaluation on the effects of anxiety of the animal during open-field test (Top). (**P*<0.05, ** *P*<0.01; compared to the non-treated CCH group). The effects of zolpidem on the anxiety level of the rat through the number of rearing during the open-field test (Below). (***P*<0.01, *** *P*<0.001; compared to the non-treated CCH group). One-way ANOVA was used to assess the effects of group. Number of animals used for each group=6.

the field (*P*<0.05), while CCH rats treated with ZPM (2.0 and 4.0 mg/kg) spent significantly less time in the center compared to untreated CCH rats (*P*<0.01, Fig. 2, Top). Additionally, the number of rearing events, a measure of exploratory and anxiety-like behavior, was significantly reduced in CCH rats treated with 2.0 mg/kg and 4.0 mg/kg ZPM compared to untreated CCH rats (*P*<0.01 for 2.0 mg/kg, *P*<0.001 for 4.0 mg/kg; Fig. 2, Below).

Morris water maze: memory acquisition during training sessions

We evaluated memory acquisition across experimental groups using a repeated two-way analysis of variance (ANOVA) over the training days, with post-hoc comparisons to the untreated CCH group. The analysis revealed significant effects of training days (*P*<0.0001) and treatment (*P*<0.0001). Additionally, significant interactions were observed between latency to reach the platform across groups over the four training days (*P*<0.05). On Day 1, no significant differences were observed between the groups (Fig. 3, Top), and all rats exhibited similar unfamiliarity with the maze. However, over the subsequent days, CCH rats displayed more pronounced learning and memory deficits, taking significantly longer to reach the platform. By Day 2, non-CCH rats demonstrated a significant improvement in platform reach time compared to untreated CCH rats (*P*<0.001), while CCH rats treated with ZPM did not show similar

 doi: 10.1538/expanim.25-0038

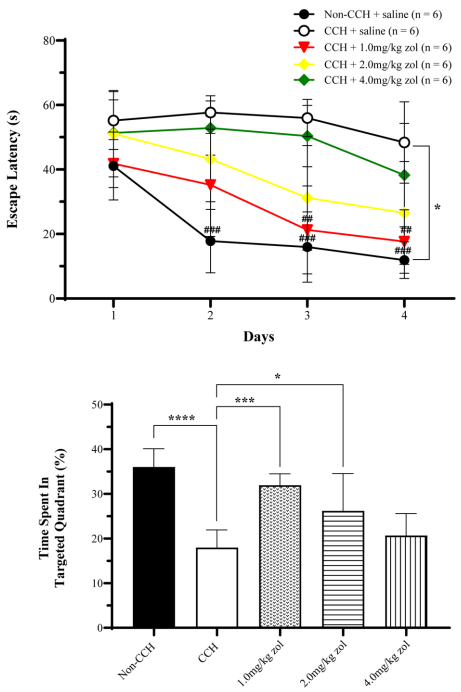

Fig. 3. The effects of CCH and zolpidem treatment on spatial memory of the rats in Morris water maze (Top). A two-way repeated measures ANOVA was used to assess the effects of group (**P*<0.05; for non-CCH versus non-treated CCH group) and day of training on latency ($^{\#\#}P$<0.01 for 1.0 mg/kg zolpidem versus non-treated CCH group; $^{\#\#\#}P$<0.001 for non-CCH versus non-treated CCH group. The effects of zolpidem on the consolidation memory of the CCH rats during probe trial of Morris water maze (Below). One-way ANOVA was used to assess the effects of group. Percentage of time spent (%) in the target quadrant southeast. (**P*<0.05, ****P*<0.001, *****P*<0.0001; compared to the non-treated CCH group). Number of animals used for each group=6.

improvements. On Day 3, CCH rats treated with 1.0 mg/kg ZPM exhibited improved spatial learning and memory, reaching the platform significantly faster (*P*<0.01). This improvement persisted through Day 4 in both the non-CCH (sham) group and CCH rats treated with 1.0 mg/kg ZPM. Additionally, CCH rats treated with 2.0 mg/kg ZPM showed a significant reduction in the time to reach the platform starting on Day 3, and this improvement was maintained through Day 4 (*P*<0.05).

Morris water maze: memory consolidation during the probe trial

We evaluated memory consolidation during the probe trial across experimental groups. Non-CCH (sham) rats spent significantly more time in the target quadrant compared to untreated CCH rats (*P*<0.0001). CCH rats treated with 1.0 mg/kg ZPM also spent significantly more time in the target quadrant compared to untreated CCH rats (*P*<0.001). Similarly, CCH rats treated with 2.0 mg/kg ZPM spent significantly more time in the target quadrant than untreated CCH rats (*P*<0.05). However, the group treated with 4.0 mg/kg ZPM showed no significant differences in time spent in the target quadrant (Fig. 3, Below).

Immunohistochemistry: expression of the ε subunit

The protein expression of GABAAR ε subunit in the CA1 and CA3 hippocampal regions was analyzed using immunofluorescence techniques, as western blot is technically challenging in these subregions due to limited tissue yield. These images were captured at 40× magnification to visualize neuronal expression (Fig. 4, Top and Middle). Quantification of the ε subunit expression, represented as raw integrated density values (a.u.), revealed a significantly higher expression in CCH rats compared to non-CCH rats (unpaired *t*-test; *P*<0.05) in both CA1 (Fig. 4, Below, Left) and CA3 (Fig. 4, Below, Right) regions. This suggests that CCH induces an upregulation of the GABAAR ε subunit in these hippocampal regions, potentially contributing to altered inhibitory signaling.

Homology modelling: sequence alignment of $GABA_AR$ subunits

The GABA(A) α1β2ε receptor was successfully modelled using human protein sequences and structural templates, with over 98% of its residues positioned within sterically favorable or allowed regions, as assessed using the Ramachandran plot [48, 49] (Supplementary Fig. 3). This high level of structural integrity underscores the reliability of the receptor model for further computational analyses. The receptor's structural organization was further characterized by detailing the sequential arrangement of each subunit within the α1β2ε complex, along with the specific residue positions for each subunit (Table 1). The pentameric assembly, in complex with ZPM and GABA molecules, is depicted to provide a comprehensive overview of its overall architecture (Supplementary Fig. 4). To evaluate sequence conservation across subunits, MSA was performed, enabling a comparative analysis of conserved and variable regions within the receptor (Fig. 5). This information is critical for understanding the subunit-specific structural and functional properties of the receptor.

Molecular docking

Targeted docking at the α1+/ε- interface yielded a binding pose with an estimated free energy of −7.2 kcal/mol. ZPM was positioned beneath α1 Loop C, adopting a more vertical orientation (Fig. 6, Top, Left). A detailed interaction summary shows that ZPM binding was primarily stabilized by van der Waals forces and hydrophobic interactions, in line with previous findings [50] (2D

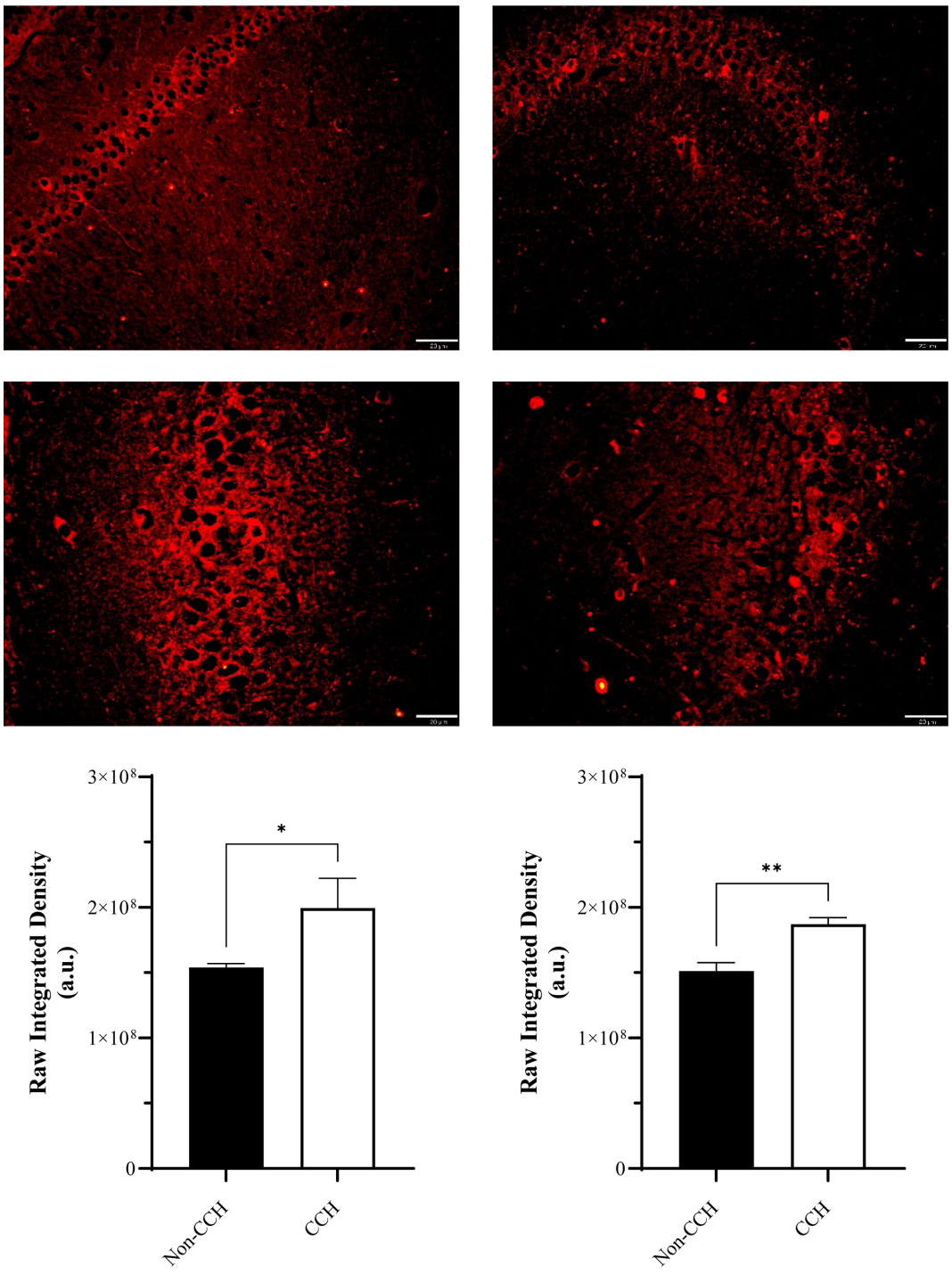

Fig. 4. Immunofluorescence images of GABAAR ε subunit expression (in red) in the CA1 (Left; Top=non-CCH, Left; Middle=CCH) and CA3 (Right; Top=non-CCH, Right; Middle=CCH) hippocampal regions. The scale bars represent 20 μm. Images were captured at 40× magnification after staining with specific antibodies. Evaluation of the GABAAR ε subunit fluorescence intensity in the hippocampal CA1 (Below, Left) and CA3 (Below, Right). Unpaired *t*-test was used to evaluate the related intensity of groups. (*P<0.05 for CA1 and ** P<0.01 for CA3 hippocampal regions; for non-CCH versus CCH rats. Number of animals used for each group=3.

Table 1. Chain and residue composition of α1β2ε

	Subunit	Residue	
	α1β2ε	First	Last
Chain A	β2	1	512
Chain B	α1	513	968
Chain C	β2	969	1,480
Chain D	α1	1,481	1,936
Chain E	ε	1,937	2,442

BIOVIA image; Supplementary Fig. 5). Key residues contributing to van der Waals interactions included α1Ser158, α1Val202, α1Thr206, ε Ser102, ε Ile234, ε Asn235, and ε Asn238, with interactions centered around ZPM's amide substituent, establishing a cohesive binding environment. Additionally, π-stacking and π-alkyl interactions were observed, involving α1Phe99, α1Tyr159, α1Tyr209, and ε Ile121. Two hydrogen bonds were also identified: ZPM's carbonyl oxygen formed a hydrogen bond with α1His101, while its imidazole nitrogen formed a hydrogen bond with α1Ser204 (Fig. 6, Top, Right; Fig. 6, Below, Left). Moreover, ε Glu233 participated in a π-anion interaction with ZPM's methylbenzene ring, potentially enhancing specificity and ligand orientation within the binding pocket (Fig. 6, Top, Right). This interaction appears to position ZPM to minimize steric clashes with bulkier residues, such as α1Phe100, α1His102, α1Tyr160, and α1Tyr210, at the pyridine methyl end.

Molecular dynamics simulation

System stability was assessed by analyzing temperature and total energy fluctuations over the simulation period. Both parameters oscillated around a relatively constant mean, indicating that the systems had reached equilibrium (Supplementary Fig. 6). An additional indicator of complex stability is the Root Mean Square Deviation (RMSD) analysis, which stabilized at approximately 70 ns, suggesting that the conformational rearrangements associated with ligand binding were complete (Supplementary Fig. 7, Left). The radius of gyration (Rg), which provides insights into protein compactness, folding stability, and conformational dynamics [51], exhibited a steady decrease until around 60 ns, after which it stabilized for the remainder of the simulation (Supplementary Fig. 7, Right). The Root Mean Square Fluctuation (RMSF) analysis revealed ligand-specific effects on receptor dynamics, particularly in regions critical for ligand binding and receptor modulation. A prominent peak was observed near residue 500, corresponding to the loop region surrounding the AB1 binding site (Supplementary Fig. 8).

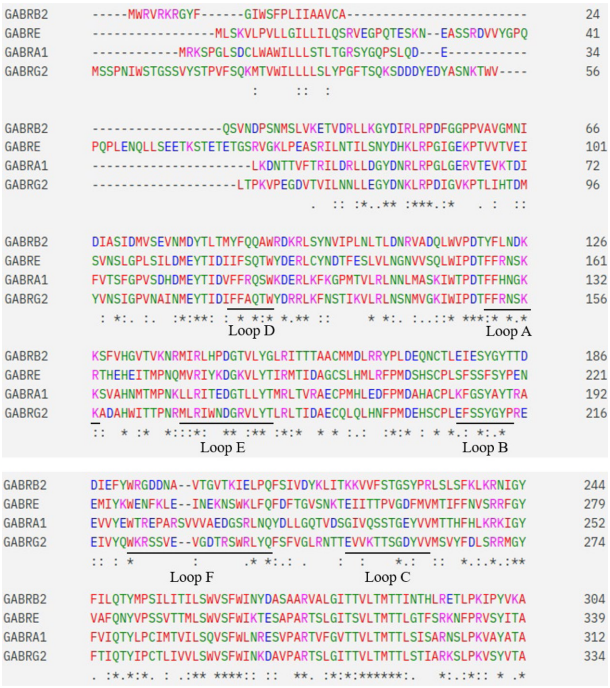

Fig. 5. Aligned amino acid sequences of each GABAAR subunit in α1β2γ2 receptor subtype. The asterisk (*) indicates fully conserved residues across all sequences at a given position, the colon (:) indicates highly conserved residues with largely similar properties, while the period (.) indicates weakly conserved residues with lower similar properties. Classically-defined neurotransmitter-binding loops (A–F) are labelled for reference.

To assess the binding affinity and stability of the receptor-ligand complex, hydrogen bond and minimum distance analyses were conducted. Hydrogen bonds were identified within a <4 Å threshold from ZPM. Throughout the 100 ns simulation, ZPM maintained consistent and sustained hydrogen bonding interactions with the receptor. Notably, ZPM primarily maintained a single hydrogen bond throughout the simulation (Fig. 6, Below, Right). This finding is further supported by minimum distance analysis, which showed that ZPM remained stably bound within 2.5 Å of the binding pocket until the end of the simulation (Supplementary Fig. 9). Additional analysis of GABA binding at site AB2 (between Chains C and D) revealed extensive hydrogen bonding and stable binding within 2 Å of the pocket for ZPM. Conversely, GABA binding at site AB1 (between Chains A and B) showed limited bonding interactions and greater displacement throughout the simulation.

Discussion

In this study, we developed an animal model of ischemic injury using PBOCCA-induced CCH. This model was chosen because it is ideal for investigating cognitive

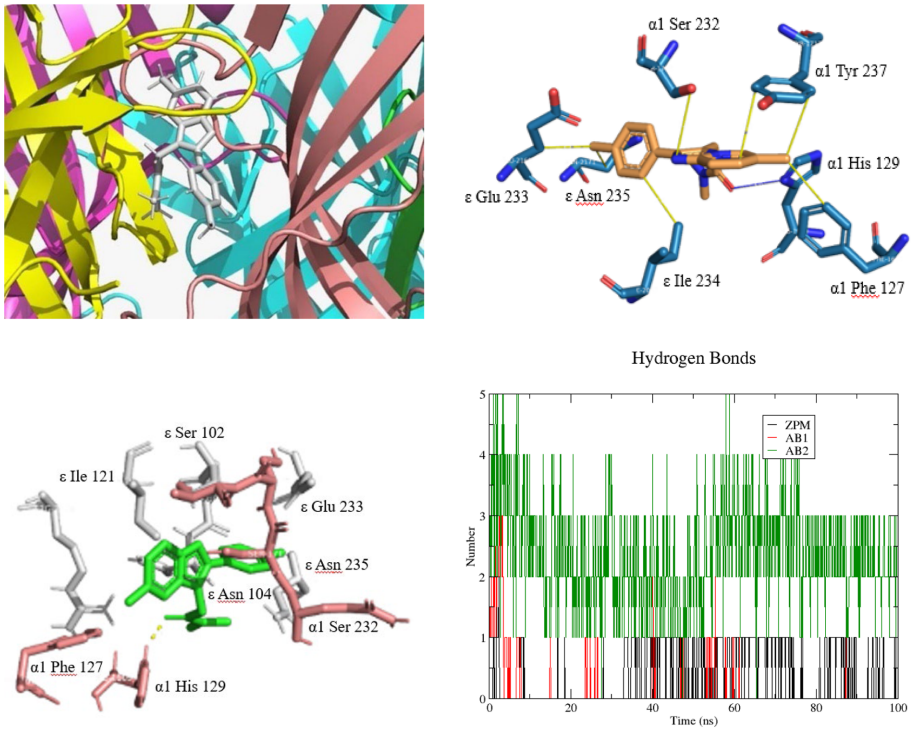

Fig. 6. A close-up view of the ligand binding site at the α1+/ε- interface (Top, Left). The α1 subunit is in yellow and the γ2 subunit is in peach. ZPM is positioned under α1 Loop C in a vertical orientation. ZPM binding within the α1+/ε- interface − interactions identified within a 4 Å radius using PLIP (Top, Right). ZPM binding within the α1+/ε- interface − interactions identified within a 5 Å radius using PyMOL (Below, Left). Hydrogen bond graphs for ZPM (black), AB1 (red) and AB2 (green) over the 100 ns simulation. ZPM demonstrated sustained hydrogen bonding with primarily a single hydrogen bond throughout the simulation. Meanwhile, AB1 displayed showed limited bonding interactions and AB2 exhibited extensive hydrogen bonding (Below, Right).

impairment in animals prior to treatment with ZPM. CCH, also known as chronic cerebral ischemia, results from sudden inadequate cerebral blood flow and is a characteristic feature of global ischemic stroke [52]. The permanent ligation of both common carotid arteries leads to a sudden reduction in cerebral blood flow to 35–45% in the cortex and hippocampus, with recovery beginning approximately one week after surgery [53]. The persistent reduction in blood flow caused by cerebral hypoperfusion has been shown to induce ischemic injury with relatively mild damage to nervous tissue and less pronounced motor dysfunction, yet it is associated with significant cognitive impairments [27]. Following the establishment of the CCH model, we subjected the animals to behavioral testing, beginning with the OFT to assess motor dysfunction. The analysis of the rats' movements included several parameters: total locomotor activity, total distance traveled, movement speed, time spent in the center of the field, and the number of rearing events. Total locomotor activity encompassed all activities recorded during the test, while total distance traveled, and movement speed provided information on the animal's motion following ischemic injury or therapeutic intervention [54]. In a novel environment, rodents typically exhibit increased caution, anxiety, and alertness to unfamiliar surroundings, preferring the periphery of the arena, a behavior known as thigmotaxis [55]. Thigmotaxis has been validated as a measure of anxiety, as it reflects the animal's tendency to remain in what it perceives as a "safer" area [54]. Additionally, the number of rearing events, where the animal stands on its hind legs, is an indicator of exploratory behavior and is often used to assess anxiety in the OFT as well as other maze tasks, such as the elevated plus maze [54, 55].

Previous studies have reported increased anxiety following CCH induction [56]. Contrary to these reports, our data showed that CCH rats spent more time in the center of the arena, suggesting an absence of anxiety. This behavior may be attributed to a state of unawareness or obliviousness to the environment. Moreover, exploratory behavior in rodents is heavily influenced by tactile sensory factors, which can be altered following surgery, leading to increased entries into the center area [57]. While there was a trend toward increased rearing in the

CCH rats compared to controls, the difference was not statistically significant. This discrepancy may be explained by factors such as the age of the animals, the methods used to induce CCH, the routes of drug administration, and the duration of the OFT [47, 57, 58]. ZPM, administered at doses of 1.0, 2.0, and 4.0 mg/kg, was tested in CCH rats using the OFT. According to [59], ZPM is rapidly absorbed, with its effects beginning within 20 min of administration. Therefore, ZPM was administered 30 min prior to the OFT to ensure maximal drug efficacy during testing. Our data demonstrated that ZPM at 4.0 mg/kg significantly reduced locomotor activity, total distance traveled, movement speed, time spent in the center, and the number of rearing events in both the center and periphery of the arena. Similar results were observed at the 2.0 mg/kg dose, except for movement speed. At 1.0 mg/kg, there were no significant differences in total distance traveled, locomotor activity, or speed. These findings are consistent with the known sedative-hypnotic properties of ZPM, which are more pronounced at higher doses [60]. As expected, the significant decrease in activity observed at the 2.0 and 4.0 mg/kg doses is likely due to the sedative effects of the drug. At the lower dose (1.0 mg/kg), the sedative effects were less prominent, which may explain the absence of significant changes in behavior. Importantly, these findings support previous research suggesting that CCH alone does not induce motor dysfunction [61]. Furthermore, ZPM's sedative effects were not associated with any alteration in the function of GABAARs. Notably, 1.0 mg/kg ZPM administration did not affect the motor function, anxiety, or exploratory behavior of CCH rats.

Since ischemic injury is known to cause significant damage to the hippocampus, the MWM has become an established method for assessing learning and memory in models of ischemic injury [62, 63]. Previous studies using the PBOCCA model have demonstrated that CCH rats exhibit impaired spatial learning and memory, as indicated by longer escape latencies and more dispersed swimming patterns [64, 65]. Consistent with these findings, our data also showed significant differences in the performance of non-CCH and CCH rats during the training and probe trials. CCH rats exhibited an initial pattern of swimming along the pool's edge, accompanied by weaving and circling, a behavior typically observed in animals with hippocampal damage [66]. These observations confirm that CCH was successfully induced in our model, resulting in cognitive impairment, and supporting the use of this model for investigating the effects of ZPM. During the MWM training sessions, CCH and non-CCH rats showed similar performance on Day 1, with both groups struggling to adapt to the task. However, by Day 2, non-CCH rats demonstrated significant improvement in platform location recognition, a trend that continued on Days 3 and 4. In the probe trial, non-CCH rats spent significantly more time in the target quadrant compared to CCH rats, indicating better memory and learning performance. This pattern suggests that CCH induction impaired spatial memory and learning in the rats.

We then assessed the effects of ZPM treatment at 1.0, 2.0, and 4.0 mg/kg on CCH rats in the MWM. On Days 3 and 4, CCH rats treated with 1.0 mg/kg ZPM demonstrated significant improvements in memory and learning, as indicated by a reduced escape latency and enhanced ability to locate the hidden platform. However, CCH rats treated with 2.0 and 4.0 mg/kg ZPM did not show significant improvements, indicating a lack of beneficial effects at these higher doses. The performance of these rats was similar to that of the non-treated CCH group. Notably, at the higher doses (2.0 and 4.0 mg/kg), the rats exhibited signs of drowsiness, consistent with the sedative properties of ZPM. In the probe trial, CCH rats treated with 1.0 mg/kg ZPM spent significantly more time in the target quadrant compared to untreated CCH rats and those treated with 2.0 or 4.0 mg/kg ZPM. The search patterns of the lower-dose ZPM group were more focused on the target quadrant, whereas the higher-dose groups exhibited scattered patterns, indicative of impaired spatial memory. These results suggest that ZPM at 1.0 mg/kg has the potential to enhance spatial learning and memory in CCH rats, whereas higher doses do not provide additional benefits and may impair cognitive function.

The paradoxical effects of ZPM in patients with brain injuries, trauma, and neurological disorders have been widely documented, with studies suggesting that these effects stem from altered GABAAR subunit expression and rearrangement [16–20, 67, 68]. In particular, the ε subunit has gained attention due to its upregulation in schizophrenia, bipolar disorder, and major depression [17] and its involvement in temporal lobe epilepsy [20]. Here, the findings of this study show a significant upregulation of the ε subunit in the hippocampal CA1 and CA3 regions of CCH rats compared to controls. The upregulation of ε subunits could play a crucial role in modulating ligand-receptor interactions, potentially leading to altered GABAergic signaling and contributing to the paradoxical effects of ZPM. As a PAM of GABAARs, ZPM's altered effects under pathological conditions may be directly linked to changes in receptor subunit composition, particularly the ε subunit, which has been associated with resistance to BZDs and altered inhibitory neurotransmission [69]. A key factor in this resistance is the fact that ε-containing GABAARs lack the γ2 sub-

unit, a critical site for BZD binding [25, 70]. This could explain the loss of BZD sensitivity in hippocampal dentate granule cells following traumatic brain injury, as observed by [19].

Further supporting this hypothesis, BZD-insensitive GABAARs have been identified in the caudal nucleus tractus solitarii, a brain region with high ε subunit expression [71]. In line with this, electroencephalography (EEG) studies revealed that, before ZPM administration, patients exhibited low frequency, synchronized brain activity, characteristic of non-REM sleep. However, after ZPM administration, brain activity transitioned to high-frequency, desynchronized patterns, resembling hippocampal and cortical firing during wakefulness [72, 73]. This shift aligns with the behavior of ε-containing GABAARs, which, upon ZPM-induced inhibitory postsynaptic currents (IPSCs), undergo deep desensitization. As a result, the decrease in open channels leads to transient hyperexcitability [26], potentially contributing to cortical arousal and improved cognitive and motor performance observed in certain neurological conditions. Additionally, studies in *Xenopus* oocytes have demonstrated that α3β1ε receptors exhibit different sensitivity to BZDs and anesthetics compared to α3β1 and α3β1γ2 receptors, giving rise to distinct effects related to sedation, stress, emotional regulation, and pain perception [74]. The regional specificity of ε subunit upregulation in CA1 and CA3 is particularly significant, as these hippocampal regions are crucial for episodic autobiographical memory, mental time travel, and autonoetic consciousness, besides being implicated in seizure susceptibility and neurodegeneration [11, 75]. Altogether, these findings reinforce the ε subunit as a key player in mediating the paradoxical effects of ZPM.

To further validate our findings, *in silico* simulations were performed to explore the structural and functional dynamics of the novel receptor-ligand interface. Homology modelling was employed to generate the ε-containing receptor, which may introduce structural constraints leading to distinct ligand-receptor interactions, potentially contributing to the paradoxical effects observed. In the γ2 subunit, the residues γ2Met57, γ2Phe77, γ2Met130, and γ2Thr142 have been identified as critical contributors to the high-affinity binding of ZPM, with γ2Phe77 and γ2Thr142 also playing a role in modulating ZPM efficacy [50, 76–79]. In contrast, in the ε subunit, residues γ2Met130 and γ2Thr142 are conserved, while γ2Met57 and γ2Phe77 are substituted with isoleucine. Mutations in γ2Phe77 have been shown to disrupt ZPM binding [76, 80]. Our findings suggest that α1Phe99 may compensate partially for γ2Phe77 as it engages in π-stacking interactions with ZPM's imidazopyridine ring, similar to interactions mediated by γ2Phe77 [2]. Nevertheless, α1Phe99 remains a crucial residue on its own, as it plays a key role in positioning α1His101 and α1Tyr159, two other crucial residues for BZD binding, within the binding pocket [80, 81]. The absence of γ2Phe77 may compromise the structural integrity of the BZD binding pocket, potentially leading to a decreased affinity for ZPM, and also affect ZPM's modulatory activity [79].

Compared to the γ subunit, sequence alignment reveals low conservation of amino acids within Loop F of the ε subunit. However, its structural dynamicity suggests that mutations in this region have minimal impact on BZD binding, as its flexibility allows other residues to compensate for the electrostatic environment of the binding pocket [78, 80, 82]. Our docking study identifies εAsn235 and εAsn238 as potential contributors to ZPM binding, with their polar amide side chains facilitating hydrogen bonds and dipole-dipole interactions. This, in turn, enables εGlu233—corresponding to γ2Glu189—to enhance electrostatic binding, contributing to strong stabilizing interactions with ZPM. While the flexibility of Loop F has little impact on the binding affinity of BZD ligands, it appears to influence their efficacy, affecting receptor modulation by acting as a transducer to link ligand binding to channel opening [83, 84]. Particularly, mutations spanning the entire region of γ2Glu182 to Arg197 impact positive modulation, whereas only Trp183 mutation significantly affects DMCM modulation [83]. Given that residues in the whole loop are poorly conserved within the ε subunit, the ε-containing receptor is expected to exhibit distinct modulatory effects in response to PAMs like ZPM.

Our docking study reveals that ZPM adopts a vertical alignment within the binding pocket, which aligns with findings from [85, 86], who first identified an allosteric relationship between the binding sites of positive allosteric modulators (PAMs). The study also identifies key residues in the α1 subunit involved in ligand binding, largely corroborating previous reports [50, 77–79, 87]. Notably, α1His101 forms strong hydrogen bonds and a salt bridge with ZPM, reinforcing its established role in high-affinity binding [2, 78]. Similarly, α1Tyr159 participated in π-alkyl interactions with ZPM, consistent with prior findings [78, 80]. However, α1Thr162 and α1Gly200, previously linked to ZPM selectivity, were not implicated in our study. Instead, we identified α1Phe99 and α1Ser158, with α1Phe99 potentially serving a role akin to γ2Phe77. The low sequence identity of α1 Loop C plays a critical role in ligand selectivity, particularly through the residues α1Ser204, α1Thr206, and α1Tyr209, which mediate differential binding af-

finities [80, 87, 88]. Our findings support previous reports, showing α1Ser204 forms a hydrogen bond with ZPM. Mutational studies further indicate that α1Ser204 affects ZPM affinity [80, 85, 87]. Meanwhile, α1Tyr209 forms π-interactions with ZPM, with mutational studies highlighting the importance of its aromatic ring for ZPM binding [2, 78, 87, 89]. Residues α1Gly200, α1Val202, and α1Ser204 have been implicated in ZPM's α1-subunit selectivity, with α1Val202 (unique to α1) likely playing a major role, as its mutation disrupts ZPM affinity [2, 80, 90]. Substitutions in the α5 subunit, such as replacing Glu200 with glycine and Thr204 with serine, enhance ZPM sensitivity, confirming these residues' role in α1 selectivity [77, 91]. However, α1Gly200 was not detected in our study, likely due to its position beyond the analysis threshold.

In parallel, extensive studies have characterized ZPM binding at the benzodiazepine-binding site located at the α1+/γ2− interface of αβγ GABAARs. Here, we briefly summarize these findings to provide context and contrast with the focus of the current study, which investigates the α1+/ε− interface in receptors containing the ε subunit. Multiple investigations, including our previous work [92], have identified a conserved set of residues involved in ZPM binding at the α1+/γ2− interface—most notably α1His102, γ2Phe77, and α1Phe100. Structural data from [2] further revealed that the pyridine methyl group of ZPM is oriented toward α1His102, while the imidazopyridine ring is positioned between α1Tyr210 and γ2Phe77, facilitating π–π stacking interactions. Additional contacts include γ2Tyr58 interacting with the acetamide group, α1Ser205 forming a hydrogen bond with the ligand's carbonyl group, and α1Thr207 engaging in hydrogen bonding with the imidazole nitrogen. Consistent with these observations, our recent unpublished study of the α1+/γ2− interface identified a complementary set of residues contributing to zolpidem binding, including γ2Met57, γ2Phe77, γ2Met130, α1Ser204, α1Ser206, and α1Thr207, aligning well with previous reports [50, 77, 78, 80]. These residues have been consistently highlighted across structural and functional studies, and despite some variation in proposed docking poses, they underscore a conserved mechanism supporting zolpidem's binding affinity and selectivity at the α1+/γ2− interface.

Molecular dynamics simulations revealed intriguing insights into ZPM's modulatory activity on ε-containing receptors, warranting further investigation. In the first 20 ns, the RMSD fluctuates significantly, suggesting an equilibration phase with early structural adjustments. Beyond 20 ns, it gradually increases and stabilizes around 74.5 Å. Minor fluctuations after 50 ns indicate some conformational flexibility, possibly due to ligand-induced rearrangements or receptor dynamics. This may reflect ZPM's ago-PAM effect by enhancing agonist responsiveness while maintaining structural stability [93]. Similarly, the Rg data show that the receptor undergoes structural relaxation and compaction during the first 50 ns, stabilizing around 51 Å in a more compact state with minor fluctuations. This is in line with the "lock and pull" mechanism where the β subunit's Loop C rotates to "lock" onto the adjacent α− interface, triggering an anti-clockwise rotation ("pull") that strengthens β+/α− interfaces, stabilizing GABA binding [94–97]. The combined RMSD and Rg analyses suggest that the system has reached equilibrium, supporting the reliability of the simulation.

Meanwhile, our RMSF data reveal a significant peak near residue 500, corresponding to the α1 subunit's extracellular loop regions surrounding the AB1 binding site. While certain loop movements are required to stabilize binding, this significant fluctuation may result from loop displacement following GABA detachment at the AB1 site. Hydrogen bond and minimum distance analyses further indicate that GABA binding at AB1 was unstable. Binding of ZPM and GABA at AB2, however, were stable. Notably, ZPM exhibited a relatively low degree of hydrogen bonding, which may promote a more flexible receptor conformation that favors activation. This aligns with [98] proposition that receptors with fewer intramolecular constraints are more likely to spontaneously adopt an active conformation. Similar trends have been observed in studies on phosphoinositide 3-kinase (PI3K) inhibitors, where strong binding and high hydrogen bond frequency are associated with receptor inhibition, enabling full occupation of active sites in dysregulated receptors for effective cancer treatment [99].

Additionally, the preferential binding of GABA at AB2 site is consistent with findings by [100], who reported that GABA exhibits a threefold higher affinity for the AB2 site compared to AB1. These distinct binding affinities may arise from subtle conformational differences between the two sites, likely influenced by the nature of their flanking subunits [100]. This is in agreement of our homology modelling results, which suggest that the poor sequence conservation of γ2 Loop F may influence the modulatory activity of PAMs. However, in this case, we are investigating the unique ε subunit, which exhibits spontaneous channel activity. While both GABA molecules are generally required for channel activation—enhancing the opening probability by 60-fold—studies have shown that channel opening can also occur with only one GABA molecule bound in the pres-

ence of a BZD agonist [100, 101]. The Monod-Wyman-Changeux (MWC) allosteric co-agonist mechanism describes how GABA-activated currents are modulated in both wild-type and spontaneously active GABAARs [101]. It also accounts for the increased frequency of channel opening in singly bound GABAARs and the direct activation of spontaneously active GABAARs by BZD agonists, a phenomenon not observed in wild-type synaptic receptors [101]. That said, despite the stable binding of only one GABA molecule in the ZPM complex, ZPM may still activate the α1β2ε receptor through its positive modulatory effect, inviting further exploration on this topic.

The central question remains: how can ZPM, a compound originally developed as a sedative-hypnotic agent, exert paradoxical effects such as promoting arousal and improving learning and memory deficits? We speculate that these effects arise from injury-induced disruptions in the balance between excitatory and inhibitory neurotransmission. In this context, ZPM may help restore homeostasis by selectively enhancing GABAergic inhibition within hyperexcitable neural circuits, thereby facilitating the reactivation of cognitive functions. A similar mechanism has been discussed by previous studies [4, 102], which suggest that the restoration of inhibitory GABAergic signaling within specific neurocircuits (mesocortical) is associated with the paradoxical effects of zolpidem. This phenomenon is likely attributable to altered expression patterns of GABAAR subunits following injury, resulting in the emergence of novel receptor subtypes—such as ε-containing GABAARs—that harbor binding sites for ZPM and constitute the primary focus of the present study. In our previous work using the *Xenopus laevis* oocyte expression system [23], we investigated α1β3ε GABAARs and identified distinct receptor populations with differential GABA sensitivity, spontaneous activity, and Zn^{2+}-mediated inhibition. These findings indicate that the ε subunit contributes to unique receptor assembly configurations and pharmacological profiles. Therefore, a comprehensive analysis of ZPM binding across different ε-containing GABAAR populations is essential to elucidate its paradoxical cognitive-enhancing effects.

Given our demonstration of ε subunit expression in the CA1 and CA3 regions of the hippocampus—areas known to be critically involved in memory formation—it remains an open question whether ε-containing GABAARs contribute significantly to cognitive processes. Another factor to consider is our recent finding that induction of status epilepticus in rat models leads to altered expression of ion transporters [103]. These transporters are essential for maintaining ionic homeostasis, particularly of Cl^-, which is critical for GABAergic signalling. This raises the question of whether the combined effects of altered ion transporter and GABAAR expression as well as alternative site for ZPM binding could contribute to cognitive improvement following brain injury. Additionally, it is possible that the resulting GABAARs contain multiple binding sites for ZPM, which may underlie a dose-dependent pharmacological response, as different receptor subtypes may be differentially activated. While preliminary findings are encouraging, the therapeutic use of ZPM for cognitive rehabilitation remains investigational. However, findings from this study suggest that low concentration of ZPM hold particular promise for therapeutic applications. Our data indicate that the neuropharmacological effects of ZPM are more distinct and pronounced at lower dose. This implies that low-dose administration may preferentially target specific receptor subpopulations, thereby eliciting the desired therapeutic effects without inducing widespread GABAergic inhibition typically associated with higher concentrations. Further research is necessary to delineate its receptor-specific targets, characterize the molecular mechanisms underlying its paradoxical effects, and evaluate its safety and efficacy in clinical studies before it can be considered a viable treatment strategy.

Conclusion

Our findings highlight the critical role of ε-containing GABAARs in mediating ZPM's paradoxical effects in brain injury. In a CCH rat model, ZPM exhibited dose-dependent effects on cognition: 1.0 mg/kg improved spatial learning and memory, while higher doses caused sedation and cognitive impairment. Immunohistochemistry showed upregulation of the ε subunit in hippocampal CA1 and CA3 regions, suggesting subunit composition changes may influence ZPM's effects. Molecular docking identified the α1+/ε− interface as a stable ZPM binding site, with key residues conserved or substituted. Molecular dynamics simulations confirmed ZPM's PAM-like behavior. The findings indicate ZPM may activate GABAARs in a singly bound state. This study underscores the α1+/ε− interface as a promising target for ZPM's effects, while calling for further research to explore ε-containing receptor subtypes and their potential in brain trauma therapy.

Acknowledgment

I would like to extend my sincere gratitude to the Ministry of Higher Education Malaysia for their financial support through the Fundamental Research Grant Scheme (FRGS) under reference code: FRGS/1/2023/SKK06/

USM/02/11. I am also deeply appreciative of Associate Professor Dr. Zurina Hassan from the Centre for Drug Research, (USM), Associate Professor Dr Wan Amir Nizam Wan Ahmad from School of Health Sciences, (USM) and Mr Muhammad Zulfadhli Othman from Department of Neurosciences (USM) for their valuable assistance, guidance, and provision of facilities for certain aspects of this study. Their support was instrumental in ensuring the successful completion of the research.

References

1. Monti JM, Spence DW, Buttoo K, Pandi-Perumal SR. Zolpidem's use for insomnia. Asian J Psychiatr. 2017; 25: 79–90 [CrossRef]. [Medline]
2. Zhu S, Sridhar A, Teng J, Howard RJ, Lindahl E, Hibbs RE. Structural and dynamic mechanisms of $GABA_A$ receptor modulators with opposing activities. Nat Commun. 2022; 13: 4582 [CrossRef]. [Medline]
3. Anderson KE, Gifeisman RI, Basting JL, Harris DJ, Rajan AR, McCall KL, et al. High prescribing and state-level variation in Z-drug use among Medicare patients. Pharmacopsychiatry. 2023; 56: 149–153 [CrossRef]. [Medline]
4. Arnts H, van Erp WS, Boon LI, Bosman CA, Admiraal MM, Schrantee A, et al. Awakening after a sleeping pill: Restoring functional brain networks after severe brain injury. Cortex. 2020; 132: 135–146 [CrossRef]. [Medline]
5. Bomalaski MN, Claflin ES, Townsend W, Peterson MD. Zolpidem for the treatment of neurologicdisorders: asystematic review. JAMA Neurol. 2017; 74: 1130–1139 [CrossRef]. [Medline]
6. Wu C, Sun D. GABA receptors in brain development, function, and injury. Metab Brain Dis. 2015; 30: 367–379 [CrossRef]. [Medline]
7. Georgiopoulos M, Katsakiori P, Kefalopoulou Z, Ellul J, Chroni E, Constantoyannis C. Vegetative state and minimally conscious state: a review of the therapeutic interventions. Stereotact Funct Neurosurg. 2010; 88: 199–207 [CrossRef]. [Medline]
8. Hahm MH, Woo J. Paradoxical Motor and Cognitive Function Recovery in Response to Zolpidem in a Patient with Hypoxic-ischemic Brain Injury: A Case Report. Clin Psychopharmacol Neurosci. 2019; 17: 453–457 [CrossRef]. [Medline]
9. Thonnard M, Gosseries O, Demertzi A, Lugo Z, Vanhaudenhuyse A, Bruno MA, et al. Effect of zolpidem in chronic disorders of consciousness: a prospective open-label study. Funct Neurol. 2013; 28: 259–264 https://www.ncbi.nlm.nih.gov/pmc/articles/PMC3951253/. [Medline]
10. Oh MK, Yoon KJ, Lee YT, Chae SW, Choi HY, Shin HS, et al. Effect of zolpidem on functional recovery in a rat model of ischemic stroke. J Int Med Res. 2018; 46: 249–257 [CrossRef]. [Medline]
11. Cherubini E, Miles R. The CA3 region of the hippocampus: how is it? What is it for? How does it do it? Front Cell Neurosci. 2015; 9: 19 [CrossRef]. [Medline]
12. Xu NZ, Ernst M, Treven M, Cerne R, Wakulchik M, Li X, et al. Negative allosteric modulation of alpha 5-containing $GABA_A$ receptors engenders antidepressant-like effects and selectively prevents age-associated hyperactivity in tau-depositing mice. Psychopharmacology (Berl). 2018; 235: 1151–1161 [CrossRef]. [Medline]
13. Mohamad FH, Has ATC. The α5-containing $GABA_A$ receptors: A brief summary. J Mol Neurosci. 2019; 67: 343–351 [CrossRef]. [Medline]
14. Ben-Ari Y. Is the awakening produced by benzodiazepines due to excitatory actions of GABA? Transl Med Commun. 2021; 6: 6. [CrossRef].
15. Che Has AT, Absalom N, van Nieuwenhuijzen PS, Clarkson AN, Ahring PK, Chebib M. Zolpidem is a potent stoichiometry-selective modulator of α1β3 GABAA receptors: evidence of a novel benzodiazepine site in the α1-α1 interface. Sci Rep. 2016; 6: 28674 [CrossRef]. [Medline]
16. Drexel M, Puhakka N, Kirchmair E, Hörtnagl H, Pitkänen A, Sperk G. Expression of GABA receptor subunits in the hippocampus and thalamus after experimental traumatic brain injury. Neuropharmacology. 2015; 88: 122–133 [CrossRef]. [Medline]
17. Fatemi SH, Folsom TD, Rooney RJ, Thuras PD. Expression of GABAA α2-, β1- and ε-receptors are altered significantly in the lateral cerebellum of subjects with schizophrenia, major depression and bipolar disorder. Transl Psychiatry. 2013; 3: e303 [CrossRef]. [Medline]
18. Kharlamov EA, Downey KL, Jukkola PI, Grayson DR, Kelly KM. Expression of GABA A receptor alpha1 subunit mRNA and protein in rat neocortex following photothrombotic infarction. Brain Res. 2008; 1210: 29–38 [CrossRef]. [Medline]
19. Mtchedlishvili Z, Lepsveridze E, Xu H, Kharlamov EA, Lu B, Kelly KM. Increase of GABAA receptor-mediated tonic inhibition in dentate granule cells after traumatic brain injury. Neurobiol Dis. 2010; 38: 464–475 [CrossRef]. [Medline]
20. Tossell K, Dodhia RA, Galet B, Tkachuk O, Ungless MA. Tonic GABAergic inhibition, via $GABA_A$ receptors containing αβƐ subunits, regulates excitability of ventral tegmental area dopamine neurons. Eur J Neurosci. 2021; 53: 1722–1737 [CrossRef]. [Medline]
21. Davies PA, Hanna MC, Hales TG, Kirkness EF. Insensitivity to anaesthetic agents conferred by a class of GABA(A) receptor subunit. Nature. 1997; 385: 820–823 [CrossRef]. [Medline]
22. Whiting PJ, McAllister G, Vassilatis D, Bonnert TP, Heavens RP, Smith DW, et al. Neuronally restricted RNA splicing regulates the expression of a novel GABAA receptor subunit conferring atypical functional properties [corrected; erratum to be published]. J Neurosci. 1997; 17: 5027–5037 [CrossRef]. [Medline]
23. Che Has AT, Hilyani Mohamad F, Othman MZ. The distinctive assembly pattern of ε subunit in ternary α1β3ε and binary β3ε GABAA receptors. J Cell Neurosci Oxid Stress. 2020; 11: 874–884 [CrossRef].
24. Davies PA, Kirkness EF, Hales TG. Evidence for the formation of functionally distinct alphabetagammaepsilon GABA(A) receptors. J Physiol. 2001; 537: 101–113 [CrossRef]. [Medline]
25. Neelands TR, Fisher JL, Bianchi M, Macdonald RL. Spontaneous and gamma-aminobutyric acid (GABA)-activated GABA(A) receptor channels formed by epsilon subunit-containing isoforms. Mol Pharmacol. 1999; 55: 168–178 [CrossRef]. [Medline]
26. Wagner DA, Goldschen-Ohm MP, Hales TG, Jones MV. Kinetics and spontaneous open probability conferred by the epsilon subunit of the GABAA receptor. J Neurosci. 2005; 25: 10462–10468 [CrossRef]. [Medline]
27. León-Moreno LC, Castañeda-Arellano R, Rivas-Carrillo JD, Dueñas-Jiménez SH. Challenges and Improvements of Developing an Ischemia Mouse Model Through Bilateral Common Carotid Artery Occlusion. J Stroke Cerebrovasc Dis. 2020; 29: 104773 [CrossRef]. [Medline]
28. Othman MZ, Hassan Z, Che Has AT. Morris water maze: a versatile and pertinent tool for assessing spatial learning and memory. Exp Anim. 2022; 71: 264–280. [CrossRef]. [Medline]
29. Palpagama TH, Sagniez M, Kim S, Waldvogel HJ, Faull RL, Kwakowsky A. $GABA_A$ Receptors Are Well Preserved in the Hippocampus of Aged Mice. eNeuro. 2019; 6: 1–13. [Medline] [CrossRef]
30. Legesse DH, Fan C, Teng J, Zhuang Y, Howard RJ, Noviello CM, et al. Structural insights into opposing actions of neuros-

teroids on $GABA_A$ receptors. Nat Commun. 2023; 14: 5091 [CrossRef]. [Medline]
31. Bollan KA, Baur R, Hales TG, Sigel E, Connolly CN. The promiscuous role of the epsilon subunit in GABAA receptor biogenesis. Mol Cell Neurosci. 2008; 37: 610–621 [CrossRef]. [Medline]
32. Šali A, Blundell TL. Comparative protein modelling by satisfaction of spatial restraints. J Mol Biol. 1993; 234: 779–815 [CrossRef]. [Medline]
33. Elias M, Liebschner D, Koepke J, Lecomte C, Guillot B, Jelsch C, et al. Hydrogen atoms in protein structures: high-resolution X-ray diffraction structure of the DFPase. BMC Res Notes. 2013; 6: 308 [CrossRef]. [Medline]
34. Morris GM, Huey R, Lindstrom W, Sanner MF, Belew RK, Goodsell DS, et al. AutoDock4 and AutoDockTools4: Automated docking with selective receptor flexibility. J Comput Chem. 2009; 30: 2785–2791 [CrossRef]. [Medline]
35. DeLano, WL. PyMOL: An open-source molecular graphics tool. CCP4 Newsletter on Protein Crystallography. 2002; 40: 82–92.
36. Salentin S, Schreiber S, Haupt VJ, Adasme MF, Schroeder M. PLIP: fully automated protein-ligand interaction profiler. Nucleic Acids Res. 2015; 43:(W1): W443–W447 [CrossRef]. [Medline]
37. Dassault Systèmes BIOVIA. (2016). Discovery Studio Modeling Environment (Version 2016) [Software]. Dassault Systèmes.
38. Lindahl E, Hess B, van der Spoel D. GROMACS 3.0: a package for molecular simulation and trajectory analysis. J Mol Model. 2001; 7: 306–317 [CrossRef].
39. Murlidaran S, Hénin J, Brannigan G. Competitive dewetting underlies site specific binding of general anesthetics to GABA(A) receptors. bioRxiv. doi: https://doi.org/10.1101/694612, July 8, 2019, preprint: not peer-reviewed. [CrossRef].
40. Kurki M, Poso A, Bartos P, Miettinen MS. Structure of POPC lipid bilayers in OPLS3e force field. J Chem Inf Model. 2022; 62: 6462–6474 [CrossRef]. [Medline]
41. Shahane G, Ding W, Palaiokostas M, Orsi M. Physical properties of model biological lipid bilayers: insights from all-atom molecular dynamics simulations. J Mol Model. 2019; 25: 76 [CrossRef]. [Medline]
42. Brannigan G, Hénin J, Law R, Eckenhoff R, Klein ML. Embedded cholesterol in the nicotinic acetylcholine receptor. Proc Natl Acad Sci USA. 2008; 105: 14418–14423 [CrossRef]. [Medline]
43. Elsagh A, Zare K, Monajjemi M. An electrochemical study of POPC phospholipid bilayers in a cell membrane. Orient J Chem. 2016; 32: 2585–2598 [CrossRef].
44. Janosi L, Gorfe AA. Simulating POPC and POPC/POPG bilayers: Conserved packing and altered surface reactivity. J Chem Theory Comput. 2010; 6: 3267–3273 [CrossRef]. [Medline]
45. Jo S, Kim T, Iyer VG, Im W. CHARMM-GUI: a web-based graphical user interface for CHARMM. J Comput Chem. 2008; 29: 1859–1865 [CrossRef]. [Medline]
46. Patodia S, Bagaria A, Chopra D. Molecular dynamics simulation of proteins: A brief overview. J Phys Chem Biophys. 2014; 4: 1–4 [CrossRef].
47. Balkaya M, Kröber JM, Rex A, Endres M. Assessing post-stroke behavior in mouse models of focal ischemia. J Cereb Blood Flow Metab. 2013; 33: 330–338 [CrossRef]. [Medline]
48. Kleywegt GJ, Jones TA. Phi/psi-chology: Ramachandran revisited. Structure. 1996; 4: 1395–1400 [CrossRef]. [Medline]
49. Wlodawer A. Stereochemistry and validation of macromolecular structures. Methods Mol Biol. 2017; 1607: 595–610 [CrossRef]. [Medline]
50. Vijayan RSK, Bhattacharyya D, Ghoshal N. Deciphering the binding mode of Zolpidem to GABA(A) α_1 receptor - insights from molecular dynamics simulation. J Mol Model. 2012; 18: 1345–1354 [CrossRef]. [Medline]
51. Sneha P, Doss CGP. (2016). Molecular dynamics: New frontier in personalized medicine. In R. Donev (Ed.), *Advances in Protein Chemistry and Structural Biology* (Vol. 102, pp. 181–224). Academic Press. [CrossRef].
52. Wang X, Yang X, Han F, Gao L, Zhou Y. Propofol improves brain injury induced by chronic cerebral hypoperfusion in rats. Food Sci Nutr. 2021; 9: 2801–2809 [CrossRef]. [Medline]
53. Otori T, Katsumata T, Muramatsu H, Kashiwagi F, Katayama Y, Terashi A. Long-term measurement of cerebral blood flow and metabolism in a rat chronic hypoperfusion model. Clin Exp Pharmacol Physiol. 2003; 30: 266–272 [CrossRef]. [Medline]
54. Seibenhener ML, Wooten MC. Use of the Open Field Maze to measure locomotor and anxiety-like behavior in mice. J Vis Exp. 2015; 96: e52434 [CrossRef]. [Medline]
55. Zimcikova E, Simko J, Karesova I, Kremlacek J, Malakova J. Behavioral effects of antiepileptic drugs in rats: Are the effects on mood and behavior detectable in open-field test? Seizure. 2017; 52: 35–40 [CrossRef]. [Medline]
56. Zhao Y, Gu JH, Dai CL, Liu Q, Iqbal K, Liu F, et al. Chronic cerebral hypoperfusion causes decrease of O-GlcNAcylation, hyperphosphorylation of tau and behavioral deficits in mice. Front Aging Neurosci. 2014; 6: 10 [CrossRef]. [Medline]
57. Prut L, Belzung C. The open field as a paradigm to measure the effects of drugs on anxiety-like behaviors: a review. Eur J Pharmacol. 2003; 463: 3–33 [CrossRef]. [Medline]
58. Kadam SD, Mulholland JD, Smith DR, Johnston MV, Comi AM. Chronic brain injury and behavioral impairments in a mouse model of term neonatal strokes. Behav Brain Res. 2009; 197: 77–83 [CrossRef]. [Medline]
59. Trenque T, Bustany P, Lamiable D, Legros S, Choisy H. Pharmacokinetics and brain distribution of zolpidem in the rat after acute and chronic administration. J Pharm Pharmacol. 1993; 1982: 611–613. [Medline]
60. Murphy HM, Ihekoronze C, Wideman CH. Zolpidem-induced changes in activity, metabolism, and anxiety in rats. Pharmacol Biochem Behav. 2011; 98: 81–86 [CrossRef]. [Medline]
61. Farkas E, Luiten PGM, Bari F. Permanent, bilateral common carotid artery occlusion in the rat: a model for chronic cerebral hypoperfusion-related neurodegenerative diseases. Brain Res Brain Res Rev. 2007; 54: 162–180 [CrossRef]. [Medline]
62. Clark RE, Broadbent NJ, Squire LR. The hippocampus and spatial memory: findings with a novel modification of the water maze. J Neurosci. 2007; 27: 6647–6654 [CrossRef]. [Medline]
63. Nikonenko AG, Radenovic L, Andjus PR, Skibo GG. Structural features of ischemic damage in the hippocampus. Anat Rec (Hoboken). 2009; 292: 1914–1921 [CrossRef]. [Medline]
64. Farkas E, Institóris A, Domoki F, Mihály A, Bari F. The effect of pre- and posttreatment with diazoxide on the early phase of chronic cerebral hypoperfusion in the rat. Brain Res. 2006; 1087: 168–174 [CrossRef]. [Medline]
65. Liu H, Zhang J. Cerebral hypoperfusion and cognitive impairment: the pathogenic role of vascular oxidative stress. Int J Neurosci. 2012; 122: 494–499 [CrossRef]. [Medline]
66. Vorhees CV, Williams MT. Assessing spatial learning and memory in rodents. ILAR J. 2014; 55: 310–332 [CrossRef]. [Medline]
67. Clauss R, Sathekge M, Nel W. Transient improvement of spinocerebellar ataxia with zolpidem. N Engl J Med. 2004; 351: 511–512 [CrossRef]. [Medline]
68. Cohen SI, Duong TT. Increased arousal in a patient with anoxic brain injury after administration of zolpidem. Am J Phys Med Rehabil. 2008; 87: 229–231 [CrossRef]. [Medline]
69. Whiting PJ. $GABA-_A$ receptor subtypes in the brain: a paradigm for CNS drug discovery? Drug Discov Today. 2003; 8: 445–450 [CrossRef]. [Medline]
70. Maksay G, Thompson SA, Wafford KA. The pharmacology of spontaneously open alpha 1 beta 3 epsilon GABA A re-

ceptor-ionophores. Neuropharmacology. 2003; 44: 994–1002 [CrossRef]. [Medline]
71. Kasparov S, Davies KA, Patel UA, Boscan P, Garret M, Paton JFR. GABA(A) receptor epsilon-subunit may confer benzodiazepine insensitivity to the caudal aspect of the nucleus tractus solitarii of the rat. J Physiol. 2001; 536: 785–796 [CrossRef]. [Medline]
72. Williams ST, Conte MM, Goldfine AM, Noirhomme Q, Gosseries O, Thonnard M, et al. Common resting brain dynamics indicate a possible mechanism underlying zolpidem response in severe brain injury. eLife. 2013; 2: e01157 [CrossRef]. [Medline]
73. Yu X, Li W, Ma Y, Tossell K, Harris JJ, Harding EC, et al. GABA and glutamate neurons in the VTA regulate sleep and wakefulness. Nat Neurosci. 2019; 22: 106–119 [CrossRef]. [Medline]
74. Ranna M, Sinkkonen ST, Möykkynen T, Uusi-Oukari M, Korpi ER. Impact of ε and θ subunits on pharmacological properties of α3β1 GABAA receptors expressed in *Xenopus* oocytes. BMC Pharmacol. 2006; 6: 1 [CrossRef]. [Medline]
75. Bartsch T, Döhring J, Rohr A, Jansen O, Deuschl G. CA1 neurons in the human hippocampus are critical for autobiographical memory, mental time travel, and autonoetic consciousness. Proc Natl Acad Sci USA. 2011; 108: 17562–17567 [CrossRef]. [Medline]
76. Buhr A, Baur R, Sigel E. Subtle changes in residue 77 of the gamma subunit of alpha1beta2gamma2 GABAA receptors drastically alter the affinity for ligands of the benzodiazepine binding site. J Biol Chem. 1997; 272: 11799–11804 [CrossRef]. [Medline]
77. Renard S, Olivier A, Granger P, Avenet P, Graham D, Sevrin M, et al. Structural elements of the gamma-aminobutyric acid type A receptor conferring subtype selectivity for benzodiazepine site ligands. J Biol Chem. 1999; 274: 13370–13374 [CrossRef]. [Medline]
78. Sancar F, Ericksen SS, Kucken AM, Teissére JA, Czajkowski C. Structural determinants for high-affinity zolpidem binding to GABA-A receptors. Mol Pharmacol. 2007; 71: 38–46 [CrossRef]. [Medline]
79. Wingrove PB, Thompson SA, Wafford KA, Whiting PJ. Key amino acids in the γ subunit of the γ-aminobutyric acidA receptor that determine ligand binding and modulation at the benzodiazepine site. Mol Pharmacol. 1997; 52: 874–881 [CrossRef]. [Medline]
80. Hanson SM, Morlock EV, Satyshur KA, Czajkowski C. Structural requirements for eszopiclone and zolpidem binding to the gamma-aminobutyric acid type-A (GABAA) receptor are different. J Med Chem. 2008; 51: 7243–7252 [CrossRef]. [Medline]
81. Xie HB, Sha Y, Wang J, Cheng MS. Some insights into the binding mechanism of the GABAA receptor: a combined docking and MM-GBSA study. J Mol Model. 2013; 19: 5489–5500 [CrossRef]. [Medline]
82. Szarecka A, Xu Y, Tang P. Dynamics of heteropentameric nicotinic acetylcholine receptor: implications of the gating mechanism. Proteins. 2007; 68: 948–960 [CrossRef]. [Medline]
83. Hanson SM, Czajkowski C. Structural mechanisms underlying benzodiazepine modulation of the GABA(A) receptor. J Neurosci. 2008; 28: 3490–3499 [CrossRef]. [Medline]
84. Khatri A, Weiss DS. The role of Loop F in the activation of the GABA receptor. J Physiol. 2010; 588: 59–66 [CrossRef]. [Medline]
85. Zhu S, Noviello CM, Teng J, Walsh RM Jr, Kim JJ, Hibbs RE. Structure of a human synaptic $GABA_A$ receptor. Nature. 2018; 559: 67–72 [CrossRef]. [Medline]
86. Bukanova JV, Kondratenko RV, Solntseva EI. Positive allosteric modulators of $GABA_A$ receptor restore chloride current from blockade by competitive antagonists in a ligand-dependent manner. J Steroid Biochem Mol Biol. 2022; 224: 106158 [CrossRef]. [Medline]
87. Buhr A, Schaerer MT, Baur R, Sigel E. Residues at positions 206 and 209 of the alpha1 subunit of gamma-aminobutyric AcidA receptors influence affinities for benzodiazepine binding site ligands. Mol Pharmacol. 1997; 52: 676–682 [CrossRef]. [Medline]
88. Wongsamitkul N, Maldifassi MC, Simeone X, Baur R, Ernst M, Sigel E. α subunits in $GABA_A$ receptors are dispensable for GABA and diazepam action. Sci Rep. 2017; 7: 15498 [CrossRef]. [Medline]
89. Richter L, de Graaf C, Sieghart W, Varagic Z, Mörzinger M, de Esch IJP, et al. Diazepam-bound GABAA receptor models identify new benzodiazepine binding-site ligands. Nat Chem Biol. 2012; 8: 455–464 [CrossRef]. [Medline]
90. Crestani F, Assandri R, Täuber M, Martin JR, Rudolph U. Contribution of the alpha1-GABA(A) receptor subtype to the pharmacological actions of benzodiazepine site inverse agonists. Neuropharmacology. 2002; 43: 679–684 [CrossRef]. [Medline]
91. Zivanov J, Nakane T, Forsberg BO, Kimanius D, Hagen WJ, Lindahl E, et al. New tools for automated high-resolution cryo-EM structure determination in RELION-3. eLife. 2018; 7: e42166 [CrossRef]. [Medline]
92. Mohamad FH, Mohamad Jamali MA, Che Has AT. Structure-function Studies of GABA(A) Receptors and Related computer-aided Studies. J Mol Neurosci. 2023; 73: 804–817 [CrossRef]. [Medline]
93. Cao AM, Quast RB, Fatemi F, Rondard P, Pin JP, Margeat E. Allosteric modulators enhance agonist efficacy by increasing the residence time of a GPCR in the active state. Nat Commun. 2021; 12: 5426 [CrossRef]. [Medline]
94. Kasaragod VB, Mortensen M, Hardwick SW, Wahid AA, Dorovykh V, Chirgadze DY, et al. Mechanisms of inhibition and activation of extrasynaptic αβ $GABA_A$ receptors. Nature. 2022; 602: 529–533 [CrossRef]. [Medline]
95. Kim JJ, Gharpure A, Teng J, Zhuang Y, Howard RJ, Zhu S, et al. Shared structural mechanisms of general anaesthetics and benzodiazepines. Nature. 2020; 585: 303–308 [CrossRef]. [Medline]
96. Kim JJ, Hibbs RE. Direct structural insights into GABAA receptor pharmacology. Trends Biochem Sci. 2021; 46: 502–517 [CrossRef]. [Medline]
97. Masiulis S, Desai R, Uchański T, Serna Martin I, Laverty D, Karia D, et al. $GABA_A$ receptor signalling mechanisms revealed by structural pharmacology. Nature. 2019; 565: 454–459 [CrossRef]. [Medline]
98. Berg KA, Clarke WP. Making sense of pharmacology: Inverse agonism and functional selectivity. Int J Neuropsychopharmacol. 2018; 21: 962–977 [CrossRef]. [Medline]
99. Arthur DE, Uzairu A. Molecular docking studies on the interaction of NCI anticancer analogues with human Phosphatidylinositol 4,5-bisphosphate 3-kinase catalytic subunit. J King Saud Univ Sci. 2019; 31: 1151–1166 [CrossRef].
100. Baumann SW, Baur R, Sigel E. Individual properties of the two functional agonist sites in GABA (A) receptors. J Neurosci. 2003; 23: 11158–11166 [CrossRef]. [Medline]
101. Rüsch D, Forman SA. Classic benzodiazepines modulate the open–close equilibrium in $\alpha^1\beta^2\gamma^{2L}$ γ-aminobutyric acid type A receptors. Anesthesiology. 2005; 102: 783–792 [CrossRef]. [Medline]
102. Schiff ND. Recovery of consciousness after brain injury: a mesocircuit hypothesis. Trends Neurosci. 2010; 33: 1–9 [CrossRef]. [Medline]
103. Othman MZ, Mohd Nasir MH, Wan Ahmad WAN, Abdullah JM, Che Has AT. Differential regulation of K^+-Cl^- cotransporter 2 (KCC2) and Na^+-K^+-Cl^- cotransporter 1 (NKCC1) expression by zolpidem in CA1 and CA3 hippocampal subregions of the lithium-pilocarpine status epilepticus rat model. Exp Anim. 2025; 74: 286–299 [CrossRef]. [Medline]